



Supplementary Materials for

Multi-omics analyses of radiation survivors identify radioprotective microbes and metabolites

Hao Guo, Wei-Chun Chou, Yunjia J. Lai, Kaixin Liang, Jason W. Tam, W. June Brickey, Liang Chen, Nathan D. Montgomery, Xin Li, Lauren M. Bohannon, Anthony D. Sung, Nelson J. Chao, Jonathan U. Peled, Antonio L. C. Gomes, Marcel R. M. van den Brink, Matthew J. French, Andrew N. Macintyre, Gregory D. Sempowski, Xianming M. Tan, R. Balfour Sartor, Kun Lu, Jenny P. Y. Ting*

*Corresponding author. E-mail: jenny_ting@med.unc.edu

Published 30 October 2020, *Science* **370**, eaay9097 (2020)
DOI: 10.1126/science.aay9097

This PDF file includes:

Materials and Methods
Captions for Tables S1 to S5
Figs. S1 to S8
References

Other Supplementary Material for this manuscript includes the following:
(available at science.sciencemag.org/content/370/6516/eaay9097/suppl/DC1)

Tables S1 to S5 (Excel files)
MDAR Reproducibility Checklist (PDF)

25 **Materials and Methods**

26 Mice

27 All animal procedures were approved (protocol #17-128/20-054) by the University of
28 North Carolina Chapel Hill (UNC) Institutional Animal Care and Use Committee
29 (IACUC) and were conducted according to US National Institutes of Health Guide for the
30 Care and Use of Laboratory Animals. Animal numbers were empirically determined to
31 optimize numbers necessary for statistical significance based on our previous reports
32 using these models (minimum of three to seven animals per group). Animals were
33 excluded if they exhibited signs of disease not associated with radiation-induced injury
34 (for example, fight wounds and malocclusion). All experiments used littermate controls,
35 or their immediate descendants. Wild-type C57BL/6J mice were obtained from Jackson
36 Laboratory and house-raised at UNC for at least nine generations. Conventionally raised
37 mice were bred and housed in specific-pathogen-free (SPF) conditions, and germ-free
38 (GF) animals were generated and housed in the National Gnotobiotic Rodent Resource
39 Center of North Carolina at Chapel Hill in AAALAC-accredited facilities.

40

41 Total body radiation

42 Total body radiation of mice was performed using an attenuator (X-302) with a
43 ¹³⁷Cesium gamma-ray irradiating source (Mark I, Model 68-1, J.L. Shepard & Associates,
44 San Fernando, CA). Alternatively, a Gammacell® 40 Exactor ¹³⁷Cesium source (Serial
45 no. 265, Best Theratronics, Ottawa, Ontario) was also used for gamma-ray irradiation,
46 with dosimetry variation of +/- 0.07 Gy as determined with phantoms by Dr. Ke Sheng,
47 UCLA, Los Angeles, CA. Non-anesthetized mice were placed in ventilated plastic pie
48 cages and exposed to 8.0 Gy-9.2 Gy total body radiation (depending on sex, age,
49 SPF/GF). Following radiation, mice were housed in sterile autoclaved cages and provided
50 standard chow and water *ad libitum* unless otherwise noted. Mice were monitored for
51 changes in body weight and other body parameters through 30 days post radiation unless
52 otherwise noted. A clinical score was determined using a cumulative scoring system (see
53 Supplementary Table S2) based on weight loss, temperature change, physical appearance,
54 posture, mobility, food consumption and hydration (*I*). Last observation carried forward
55 (LOCF) method was used when interpreting the clinical score plots. Immediate
56 indications for euthanasia included: weight loss greater than 25% of starting body weight,
57 unconsciousness, an inability to remain upright, agonal respiration (gaspings) or
58 convulsions.

59

60 Histopathology

61 To assess tissue pathology, spleens, femurs, small intestines and colons were collected
62 and fixed in 10% neutral-buffered formalin, paraffin-embedded, and sectioned (4-micron
63 thickness) at the UNC Lineberger Animal Histopathology Core Facility. Prior to paraffin-
64 embedding, femurs underwent an additional decalcification step in Immunocal™
65 (StatLab, McKinney, TX). Slides were stained with hematoxylin and eosin (H&E) and
66 semi-quantitatively scored by a board-certified pathologist (N.D.M.), who was blinded to
67 experimental conditions. Histology was performed using an Olympus BX43 microscope
68 with Olympus objective UPlanFL N 20X (na = 0.17). Images were taken with a DP27
69 camera and CellSens Dimension 1.16 software (Olympus). For all microscopic studies,

70 evaluation was performed at ambient temperature. Image processing was limited to
71 contrast adjustment and sharpening and was performed using Adobe Photoshop CS4
72 v11.0.2 (Adobe, San Jose, CA). Histology scores represent the sum of each histological
73 alterations as outlined below.

74 Spleen scoring system was based on the amount and patterns of extramedullary
75 hematopoiesis (EMH) as described here: (1) atrophy; (2) atrophic white pulp with less
76 than 20% EMH; (3) atrophic white pulp with 20-60% EMH; (4) atrophic white pulp with
77 60-100% EMH; (5) early white pulp recovery with extensive EMH in red pulp; (6) well-
78 developed white pulp with extensive EMH in red pulp; (7) normal spleen.

79 Femur scoring system was based on the overall percentage of marrow space occupied
80 by hematopoietic cells as compared to adipocytes and expressed as percent bone marrow
81 cellularity [(marrow space occupied by hematopoietic cells/total marrow space) ×
82 ~100%].

83 Slides of spleen and femur sections were also stained with Ki67 antibody (Cell
84 Signaling, #12202) or cleaved caspase 3 antibody (Cell Signaling, #9661).
85

86 Bone marrow stem cells isolation

87 Bone marrow stem cells were obtained using the magnetic cell sorting (MACS)
88 system (Miltenyi Biotec) according to manufacturer's protocols. Briefly, bone marrow
89 cells were collected from the femur and tibia of mice and then incubated with CD117
90 MicroBeads (Miltenyi Biotec, #130-091-224) for 15 minutes in the refrigerator (2–8 °C).
91 After washing with buffer, cells were resuspended in 500 µL of buffer and applied to
92 MACS column. Columns were washed with the appropriate buffer and then placed on a
93 suitable collection tube, where magnetically labeled cells were flushed off. The purity of
94 the CD117⁺ cells collected by the MACS was around 90%, and the viability was around
95 99%. These purified CD117⁺ cells were used in immunoblotting or ROS detection assay.
96

97 Intestinal epithelial cell (IEC) and intestinal intraepithelial lymphocyte (IEL) isolation

98 Colons were harvested from mice and cut open longitudinally. Feces were removed
99 by swishing the tissue in a 100 cm dish containing ice-cold PBS. Tissues were washed
100 again in a separate dish containing PBS and cut into small pieces. After transferring to 50
101 mL tubes containing PBS and shaken vigorously by hand, samples were washed with
102 PBS, until no bubbles appeared. Tissue pieces were then transferred into 5 ml Digestion
103 buffer (100 µl DNase (1/50, Sigma, #DN25-1G), 20 µl Collagenase D (1/250, Roche,
104 #11088874103), 100 µl Dispase (1/50, Stemcell, #07913)). Samples were minced well
105 with scissors and transferred into new 50 ml tubes followed by shaking at 37 °C for 30
106 min. Then, samples were further shaken vigorously for 2 minutes by hand. Homogenates
107 were supplemented with 14 mL complete RPMI and the digestion mixture was passed
108 through a 100 µm cell strainer. Cells were washed with 10 ml complete RPMI and the
109 pellets contained both IEL and IEC, which were used in immunoblot assay.
110

111 ROS detection

112 Intracellular ROS levels in bone marrow stem cells were detected using DCFDA
113 Cellular ROS Detection Assay Kit (abcam, #ab113851) according to manufacturer's
114 protocol. Briefly, cells were washed once in 1X Buffer and then incubated with 25 µM
115 DCFDA for 45 min at 37 °C. Cells were then washed with 1X Buffer and placed in 96-

116 well plate for fluorescent reading at Excitation/Emission settings of 485/535 nm. The
117 average level of ROS in non-radiation naïve group was calculated, and all samples'
118 results were normalized to this average.

119

120 Fecal DNA extraction, 16S rRNA gene sequencing and data analysis

121 Fecal sample preparation and 16S rRNA sequencing were conducted as previously
122 described (11, 42). Briefly, fecal samples were collected, snap-frozen and stored at -80°C.
123 DNA was isolated by incubating fecal material at 65 °C for 30 min in Lysing Matrix E
124 tubes (MP Biomedicals, #6913-100) containing 200 mM NaCl, 100 mM Tris, 20 mM
125 EDTA (pH 8.0), SDS and proteinase K (Qiagen). Phenol: Chloroform: Isoamyl alcohol
126 (Invitrogen) was added, and samples were homogenized at 4 °C for 3 min using a bead
127 beater homogenizer followed by a centrifugation at 8000 rpm for 3 min at 4 °C.
128 Supernatants were incubated with Phenol: Chloroform (Invitrogen) for 10 min at room
129 temperature. Samples were then centrifuged at 13,000 rpm for 5 min at 4 °C, and aqueous
130 phases were incubated with isopropanol and 3 M sodium acetate (pH 5.2) at -20 °C
131 overnight. The precipitated DNA was collected by centrifugation at 13000 rpm at 4 °C
132 for 20 min, washed twice with 100% cold ethanol and resuspended in TE buffer. DNA
133 was further purified using a DNeasy Blood and Tissue Kit (Qiagen, #69504) according to
134 the manufacturer's protocol.

135 Fecal DNA samples were amplified by PCR using barcoded primer pairs targeting the
136 V1-V2 or V3-V4 region of the 16S rRNA gene. PCR amplicons were sequenced using
137 the Mi-Seq Illumina sequencer. The resulting bacterial sequence fragments were
138 clustered into Operational Taxonomic Units (OTUs) and aligned to Greengenes microbial
139 gene database with 97% sequence similarity in QIIME (1.8.0). Bacterial taxonomy
140 summarization, rarefaction analyses of microbial diversity, compositional differences
141 (with dissimilarity value indicated by Unweighted UniFrac Distance) were calculated in
142 QIIME as previously described using scripts (including `pick_open_reference_otus.py`,
143 `summarize_taxa.py`, `alpha_rarefaction.py`, `jackknifed_beta_diversity.py` and
144 `make_distance_boxplots.py`) (11). PCA plots were generated by QIIME script
145 (`make_2d_plots.py`). Heatmap was generated based on normalized bacteria abundance
146 using a R function `heatmap` (a function in R `stats`). Specifically, we first removed bacteria
147 which have zero or very low abundance (total abundance across samples < 0.000165) in
148 all samples. This reduced the total number of bacteria from 172 to 81. For the remaining
149 81 bacteria, we sorted them by t-test statistics (to test abundance between the elite-
150 survivors and controls). To enhance the contrast, we used by-row (by bacteria)
151 normalized values of relative abundance to generate the heatmap.

152

153 SCFAs detection by GC-MS quantitation

154 Authentic reference standards of acetic acid (AA), propionic acid (PA), and butyric
155 acid (BA) were obtained from Sigma-Aldrich (St. Louis, MO, USA). Stable isotope
156 labelling d4-AA, d2-PA and d2-BA were obtained from CDN Isotopes (Pointe-Claire,
157 Quebec, Canada). HPLC-grade hexane and water were purchased from Thermo Fisher
158 Scientific (Waltham, MA, USA), whereas propyl chloroformate (PCF), pyridine (Py), 1-
159 propanol (PrOH), as well as semiconductor-grade sodium hydroxide (NaOH) and
160 anhydrous sodium sulfate (Na₂SO₄), were purchased from Sigma-Aldrich (St. Louis, MO,
161 USA).

162 Fecal SCFA contents were quantified as described in Zheng *et al.* (43) with
163 modifications. For each fecal sample, ~40 mg aliquots were extracted on a TissueLyzer
164 (Qiagen, Hilden, Germany) with 0.005 M NaOH solution containing 50 µg/mL of d4-AA,
165 10 µg/mL of d2-PA, and 10 µg/mL of d2-BA, followed by 20 min centrifugation at
166 13,200 rpm. The supernatant layers were transferred to glass tubes and derivatized by
167 subsequently adding water, PrOH:Py (3:2, v/v) and PCF. Two-minute sonication was
168 then performed, and the propyl derivatives were extracted twice with hexane, combined
169 and transferred to Na₂SO₄-containing autosampler vials for GC-MS quantitation. The
170 instrumental analysis was conducted on an Agilent 7820A GC-5977B MSD system
171 (Santa Clara, CA, USA), where one-microliter extracts were injected under 1:10 split
172 mode, ionized with an electron ionization source, and separated by an Agilent DB-5
173 column (30m x 0.25mm x 0.25 µm) (Santa Clara, CA, USA) with 1 mL/min helium
174 flowing through the column. The temperature program was as follows: initial oven
175 temperature held at 50 °C for 2 min, ramped to 70 °C by 10 °C/min, to 85 °C by 3 °C/min,
176 to 110 °C by 5 °C/min, to 290 °C by 30 °C/min, and finally held at 290 °C for 8 min. The
177 relative standard deviations of both intra- and inter-day precision of analysis were below
178 10%. Limits of quantitation was determined to be 1 ng on column for AA, 1 ng for PA
179 and 0.1 ng for BA.

180

181 Untargeted metabolomics

182 LC-MS grade solvents including water, methanol, acetonitrile, and formic acid were
183 purchased from Thermo Fisher Scientific (Waltham, MA, USA). Untargeted
184 metabolomics of mouse feces was performed on a high-resolution accurate mass (HRAM)
185 mass spectrometry-based platform coupling to a cutting-edge integrated
186 chemoinformatics pipeline as modified from a previous publication (22). Untargeted
187 metabolomic profiling of mouse feces was conducted on a LC-MS platform. The system
188 consisted of a Vanquish UHPLC and a Thermo Scientific Q-Exactive high resolution
189 /accurate mass spectrometer interfacing with a heated electrospray ionization (HESI)
190 source and a hybrid quadrupole-orbitrap mass analyzer operated at 70,000 mass
191 resolution (Waltham, MA, USA). For each sample, ~25 mg feces was aliquoted, shake-
192 extracted by ice-cold methanol:water (1:1, v/v) and centrifuged at 12,000 rpm for 10 min.
193 The supernatants were dried in a vacuum concentrator (Waltham, MA, USA) and
194 resuspended in acetonitrile:water (2:98, v/v) upon instrumental analysis. Extracts of
195 equivalence to 0.125 mg raw feces were injected and subject to a chromatographic
196 separation using a C18 column (Waters Acquity UPLC HSS T3, 2.1 mm × 100 mm, 1.7
197 µm) (Milford, MA, USA). The mobile phases consisted of 0.1% formic acid in water
198 (“A”) and 0.1% formic acid in acetonitrile (“B”) and the LC eluents were run at a
199 constant flow rate of 0.4 mL/min under 40 °C, following the gradient: 2% B, 0-2 min; 2%
200 B to 80% B, 2-11 min; 80% B to 98% B, 11-12 min; 98% B, 12-16 min; 98% B to 2% B,
201 16-16.1 min; 2% B, 16.1-20 min. The HESI ion source conditions were as follows: sheath
202 gas flow rate, 60 L/min; aux gas flow rate, 10 L/min; sweep gas flow rate, 1 L/min; spray
203 voltage, 2.75 kV; capillary temperature, 325 °C; aux gas heater temperature, 400 °C.
204 Stringent quality assurance (QA) /quality control (QC) procedures were applied,
205 including timely mass calibration, sample randomization, and intermittent QC injection.

206 All MS1 raw data were processed in XCMS (Scripps, La Jolla, CA) for peak picking,
207 peak alignment, gap filling and sample normalization. Univariate Welch's t-test and
208 multivariate principal component analysis (PCA) were applied to screen for ion features
209 of distinct group differences. For ion features of top 500 largest fold changes or of
210 potential microbial relevance, MS/MS spectral data in fullscan plus parallel reaction
211 monitoring (PRM) hybrid mode were collected and fed to a cutting-edge
212 chemoinformatic pipeline that integrates empirical MS/MS database search and in-silico
213 structural dereplication. Compound identification was implemented in MS-DIAL 2.94
214 and MS-FINDER 3.12, with four analytical metrics (i.e. accurate mass, isotopic
215 abundances, tandem mass spectra and retention time) imported to boost annotation
216 confidence while reducing scoring bias. All identifications were manually curated and
217 validated as available using an in-house metabolomic database established based on
218 authentic chemical standards. Confidence level of annotation was assigned to each
219 structure as required by the Metabolomics Standards Initiative (MSI). For pathway
220 analysis and visualization, MetaboAnalyst 4.0 was used to perform metabolite
221 enrichment analysis (MSEA) and create a heatmap showing a select of 50 annotated
222 structures with largest group difference; a MetaMapp approach was used to compute a
223 metabolomic network clustering by biochemical and chemical relationship that was
224 further visualized in CytoScape 3.7.1.

225

226

227

228

229

230

231

232

233

234

235

236

237

238

239

240

241

242

243

Fig. S1.

Gut microbiota from elite-survivors attenuate radiation-induced disease. SPF C57BL/6 mice passively received microbiota exchange via dirty cage sharing followed by a high dose of total body radiation as shown in Fig 1E. Femurs and spleens were obtained from recipients at day 30 post radiation and stained for H&E (**A**), cleaved caspase 3 (**B**) and Ki67 (**C**). In (**A**), white pulp (WP, black dash circles), red pulp (RP, areas between black solid lines), granulopoiesis (yellow dash circle), and megakaryocytes (black arrows) are shown. Bone marrow cellularity and spleen extramedullary hematopoiesis (EMH) scores were quantified (see Method). (**D**) Spleens were collected at day 30 post radiation. Cleaved caspase 3 protein levels were detected by western blot. A.U., arbitrary units. Each lane and symbol represent one mouse. Figures represent or are pooled from two-three independent experiments. Error bars show SEM, ** $p < 0.01$, *** $p < 0.001$, **** $p < 0.0001$ determined by Mann-Whitney test (A, D).

Fig. S2

Fecal microbiota transplant protects against radiation-induced injury and death. (A)

Illustration of FMT experiment in SPF C57BL/6 mice. **(B)** Survival rates and **(C)** clinical scores were monitored for 30 days post total body radiation. Fractions indicate the number of mice that survived to the end of the experiment. Figures represent pooled data from three independent experiments. **(D)** Mice were euthanized at day 12 post radiation. Femurs and spleens were stained for H&E and quantified for bone marrow cellularity and spleen extramedullary hematopoiesis (EMH) scores. Focal hematopoiesis (yellow arrows and area within yellow solid lines) and lymphocyte depleted follicles (area within black dashed lines) are shown. Each symbol represents one mouse. Error bars show SEM, ** $p < 0.01$, *** $p < 0.001$ determined by log-rank (Mantel Cox) test (B) and Mann-Whitney test for area under the curve (AUC) (C).

Fig. S3

Bacteria strains that were reduced in elite-survivors do not show any radioprotection. SPF C57BL/6 mice received antibiotics treatment followed by *Staphylococcus aureus*, *Staphylococcus saprophyticus*, *Streptococcus agalactiae*, *Lachnospiraceae* (Lachno, a mixture of 23 individual strains in the family *Lachnospiraceae*) or media control (BHI) administration twice a week for eight weeks. A high dose of total body radiation was conducted. **(A)** Survival rates and **(B)** clinical scores were monitored for 30 days post radiation. Fractions indicate the number of mice that survived to the end of the experiment. Figures represent pooled data from three independent experiments. Each symbol represents one mouse. Error bars show SEM, * $p < 0.05$, *** $p < 0.001$ determined by log-rank (Mantel Cox) test (A) and Mann-Whitney test for area under the curve (AUC) (B).

Fig. S4

***Lachnospiraceae* does not promote tumor growth nor does it interfere with the efficacy of radiotherapy.** (A) Illustration of *Lachnospiraceae* administration in tumor models. SPF C57BL/6 mice received antibiotics treatment followed by *Lachnospiraceae* (Lachno) or media control (BHI) administration twice a week for eight weeks. Then, melanoma cell line (B16) or lymphoma cell line (EL4) were subcutaneously injected into recipients' abdomen. (B-C) Tumor volumes were monitored and calculated by $\text{length} \times \text{length} \times \text{width} / 2$. (D) Illustration of *Lachnospiraceae* administration in tumor radiotherapy models. SPF mice received antibiotics treatment followed by *Lachnospiraceae* (Lachno) or media control (BHI) administration twice a week for eight weeks. Then, melanoma cell line (B16) was subcutaneously injected into recipients' abdomen. Ten days later, tumor site localized radiation (10 Gy) was conducted. (E) Survival rate and (F) Tumor volumes ($\text{length} \times \text{length} \times \text{width} / 2$) were monitored. (G) Tumor growth in each individual mouse was shown. Figures represent or are pooled from two-three independent experiments. Each symbol represents one mouse. Error bars show SEM, n.s. not significant, ** $p < 0.01$ determined by log-rank (Mantel Cox) test (E) and Mann-Whitney test for area under the curve (AUC) (F).

Fig. S5

Short chain fatty acid levels are increased in elite-survivors or ES-Recipients as detected by GC-MS. Acetate, butyrate, propionate and total SCFAs levels in the fecal materials were determined by Mass Spectrometry from **(A)** controls (n=6) and elite-survivors (n=8-12) groups or from **(B)** recipient groups of dirty cage sharing experiment (Ctrl-Recip, n=7; ES-Recip, n=8) described in Fig. 2A. Fecal samples were collected from two independent experiments. Each symbol represents one mouse. Error bars show SEM, n.s., not significant, *p<0.05, determined by Mann-Whitney test.

Fig. S6

The efficiency of *Lachnospiraceae* radioprotection depends on SCFA production. (A-B) 23 individual strains in the family *Lachnospiraceae* were cultured separately and the SCFAs levels in the culture medium were detected by mass spectrometry. Three strains (No. 8, 9, 21) that produced low levels of SCFAs were referred to as Lachno-SCFA low producer; while three strains (No. 2, 14, 20) that produced high levels of SCFAs were referred to as Lachno-SCFA high producer. Although strain No. 7 and 10 produced high levels of SCFAs, we didn't choose them because they grew extremely slowly in vitro. **(B)** The butyrate and propionate production from these two groups are shown. **(C)** Illustration of Lachno-SCFA low/high producer treatment in SPF C57BL/6 mice. **(D)** Survival rates and **(E)** clinical scores were monitored for 30 days post total body radiation. Error bars show SEM, * $p < 0.05$, **** $p < 0.0001$ determined by log-rank (Mantel Cox) test (D) and Mann-Whitney test for area under the curve (AUC) (E).

Fig. S7

Radiation-induced DNA damage is attenuated by SCFAs treatment. SPF C57BL/6 mice received 200 mM acetate-, butyrate- or propionate-containing drinking water for eight weeks followed by a high dose of total body radiation. Primary intestinal epithelial cell (IEC) and intestinal intraepithelial lymphocyte (IEL) were isolated from indicated groups (N: naïve; B: butyrate; P: propionate; C: control) at 24h post radiation. Phosphorylated and total p53 and 53BP1 were detected by western blot.

Fig. S8

Metabolic alterations between age-matched controls and elite-survivors by untargeted metabolomics. Metabolite profiles were measured in fecal samples from controls and elite-survivors at day 290 post total body radiation. **(A)** Hierarchical clustering heatmap representing 50 highly changed metabolites of distinct group patterns are shown. **(B)** Relative abundance of selected tryptophan metabolites. Each symbol represents one mouse. Error bars show SEM, * $p < 0.05$, ** $p < 0.01$ determined by Student's t test.

Table S1.

Bacterial taxa list in heatmap analysis compared between elite-survivors and age-matched controls. (separate file)

Table S2.

Clinical score parameters for radiation induced sickness. (separate file)

Table S3.

Leukemia patients' information. (separate file)

Table S4.

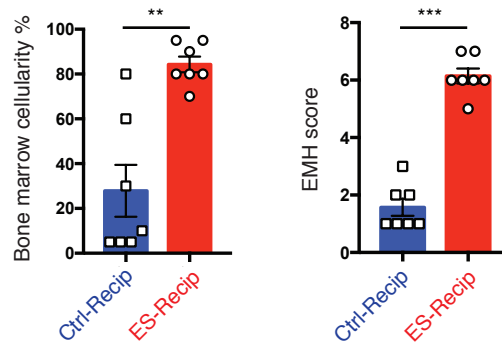
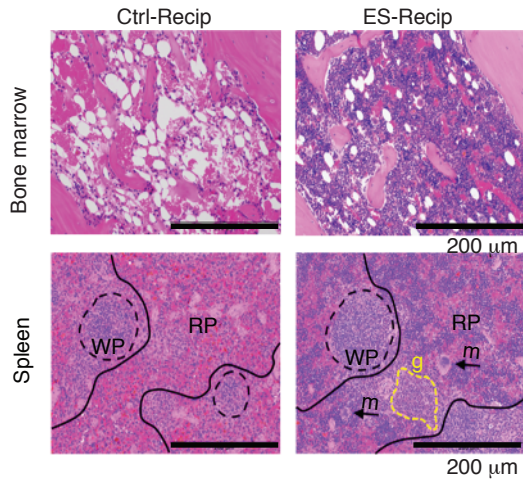
A list of metabolites assayed and analyzed with significant difference between age-matched controls and elite-survivors (Wech's t-test, $P < 0.05$, fold change > 1.2). (separate file)

Table S5.

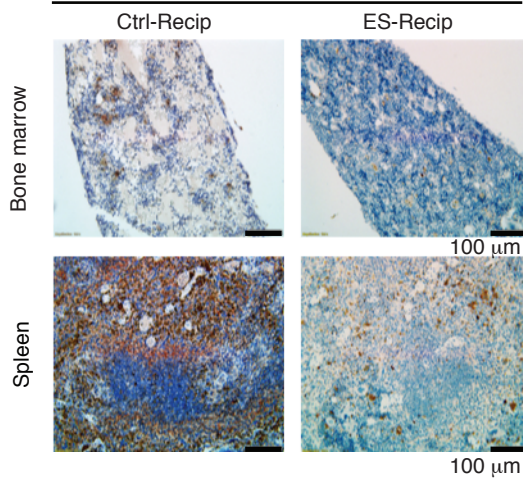
A list of 141 unique metabolites that showed difference between age-matched controls and elite-survivors, detailing correlations between metabolomics data and community metabolic potential scores and potential taxonomic contributors. (separate file)

A

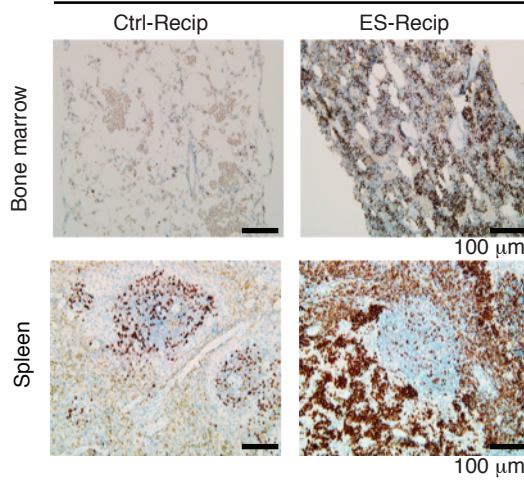
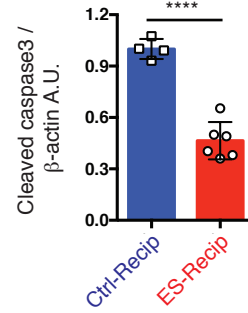
H&E

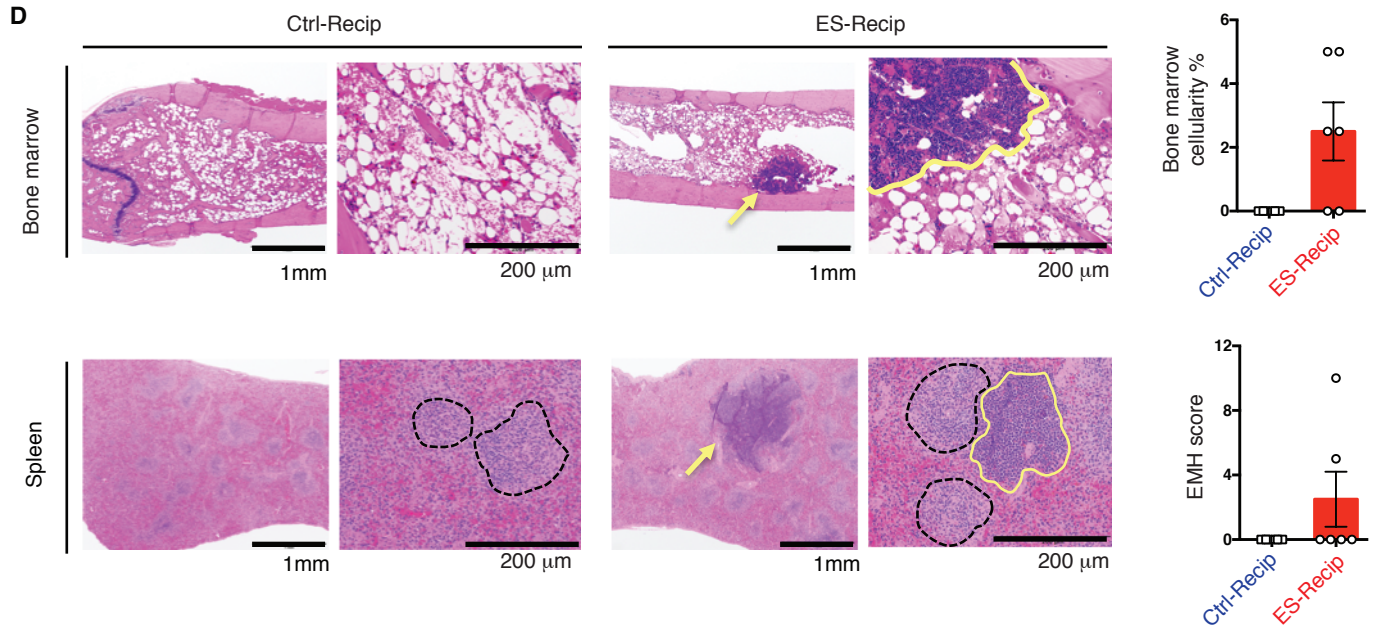
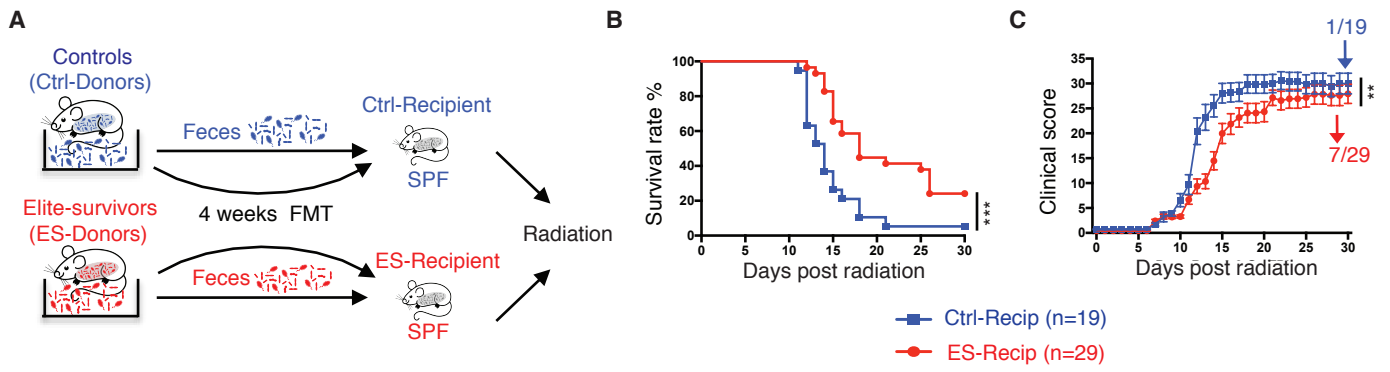
**B**

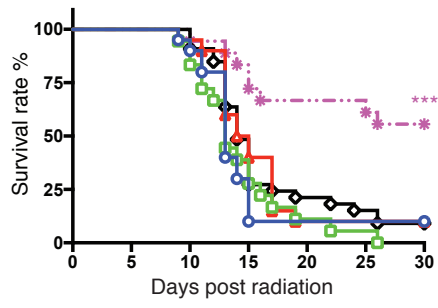
Cleaved caspase 3

**C**

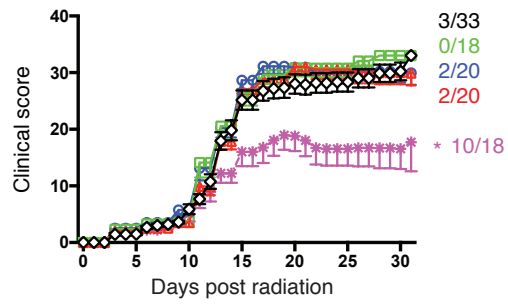
Ki67

**D**

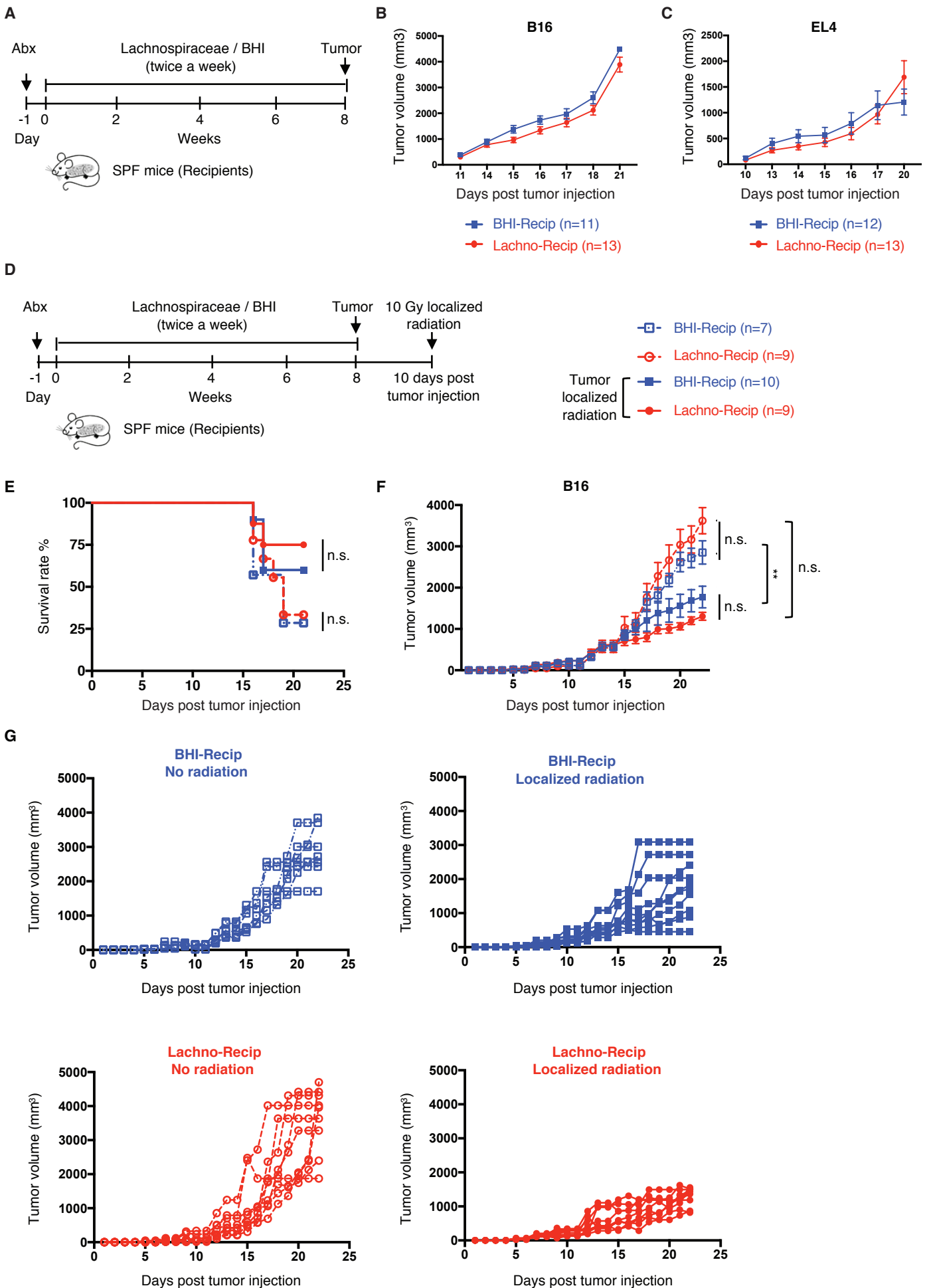


A

- ◆ BHI (n=33)
- ◆ *Lachnospiraceae* (n=18)
- ◆ *Staphylococcus aureus* (n=20)
- ◆ *Staphylococcus saprophyticus* (n=18)
- ◆ *Streptococcus agalactiae* (n=20)

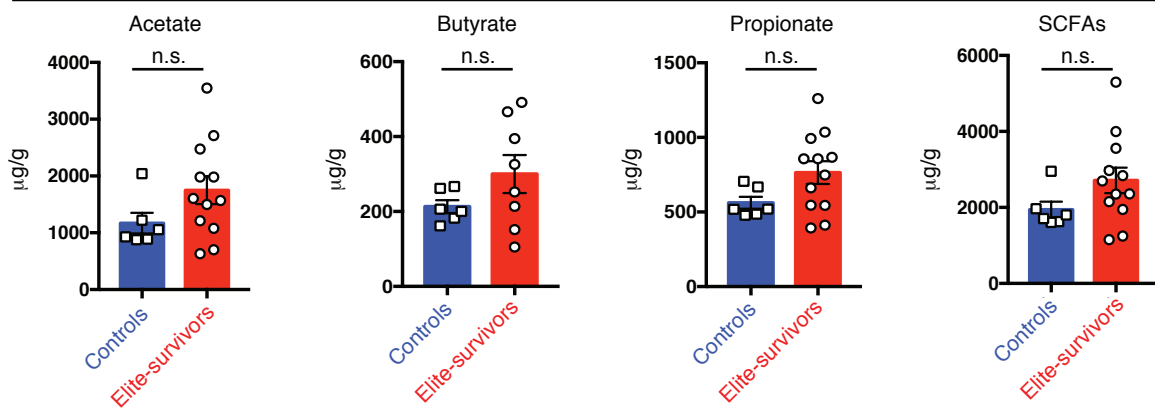
B

- 3/33
- 0/18
- 2/20
- 2/20
- * 10/18

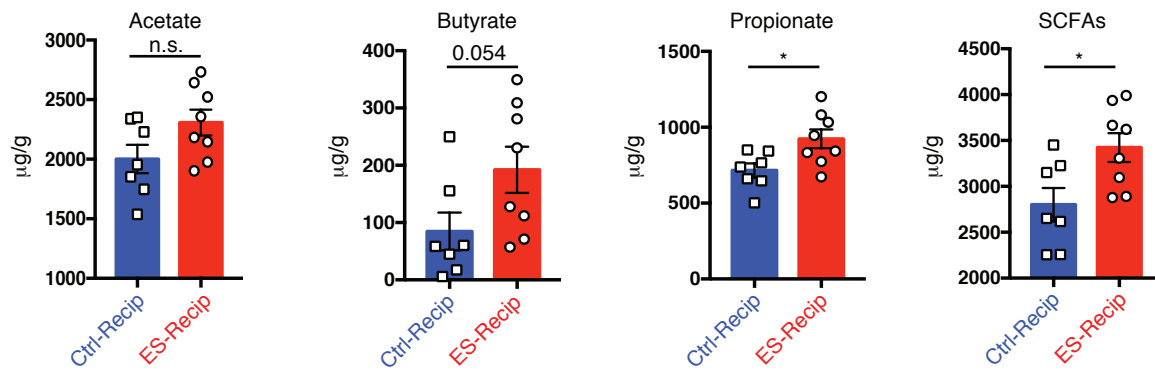


A

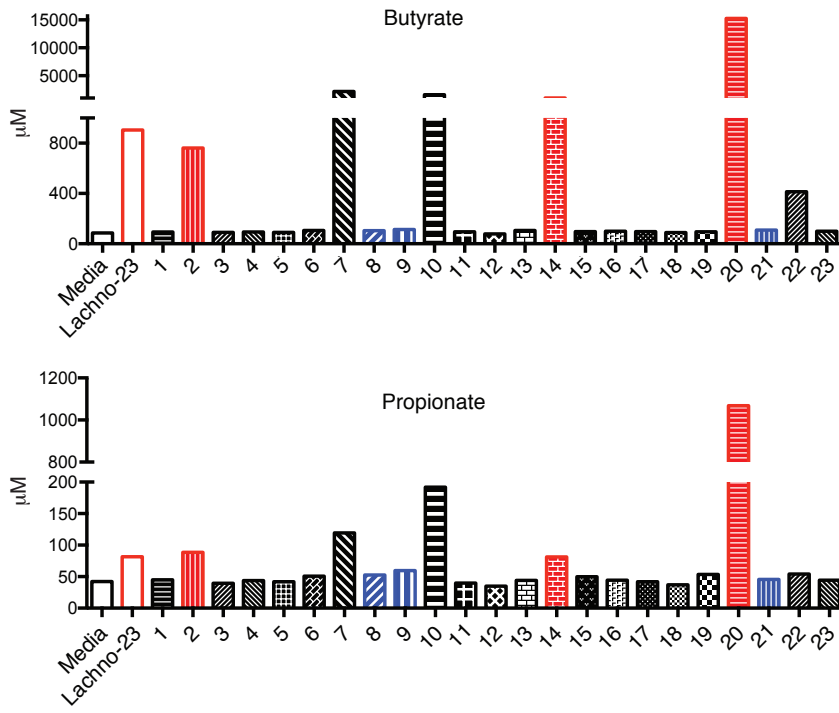
Age-matched controls vs. elite-survivors

**B**

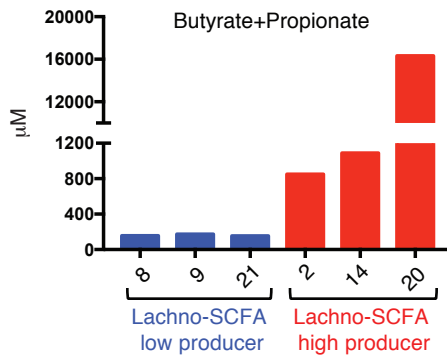
Dirty cage sharing expt.



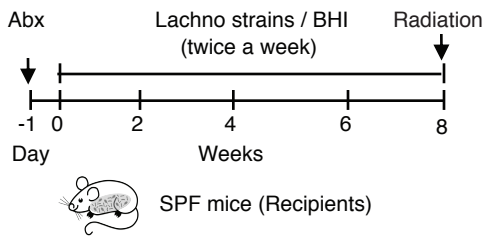
A



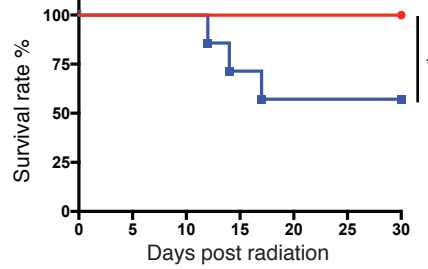
B



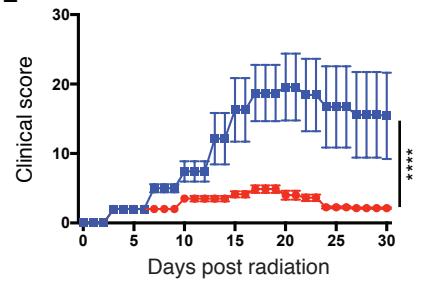
C



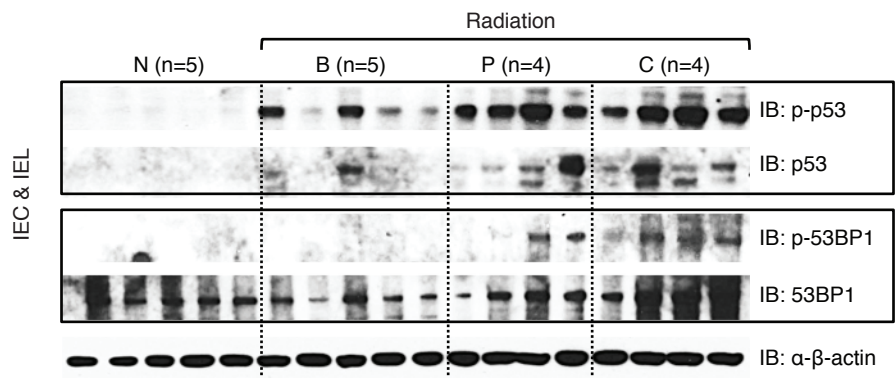
D



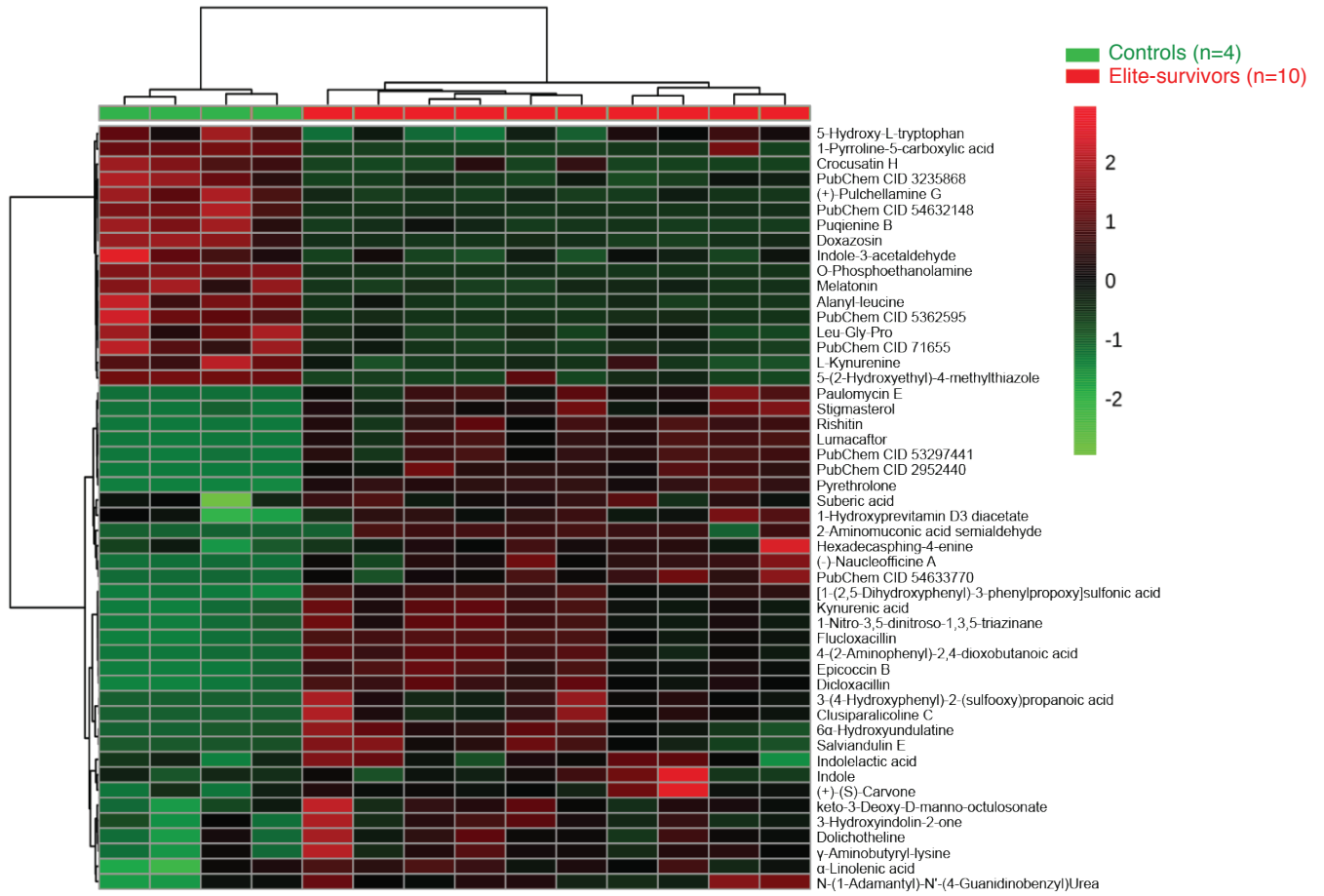
E



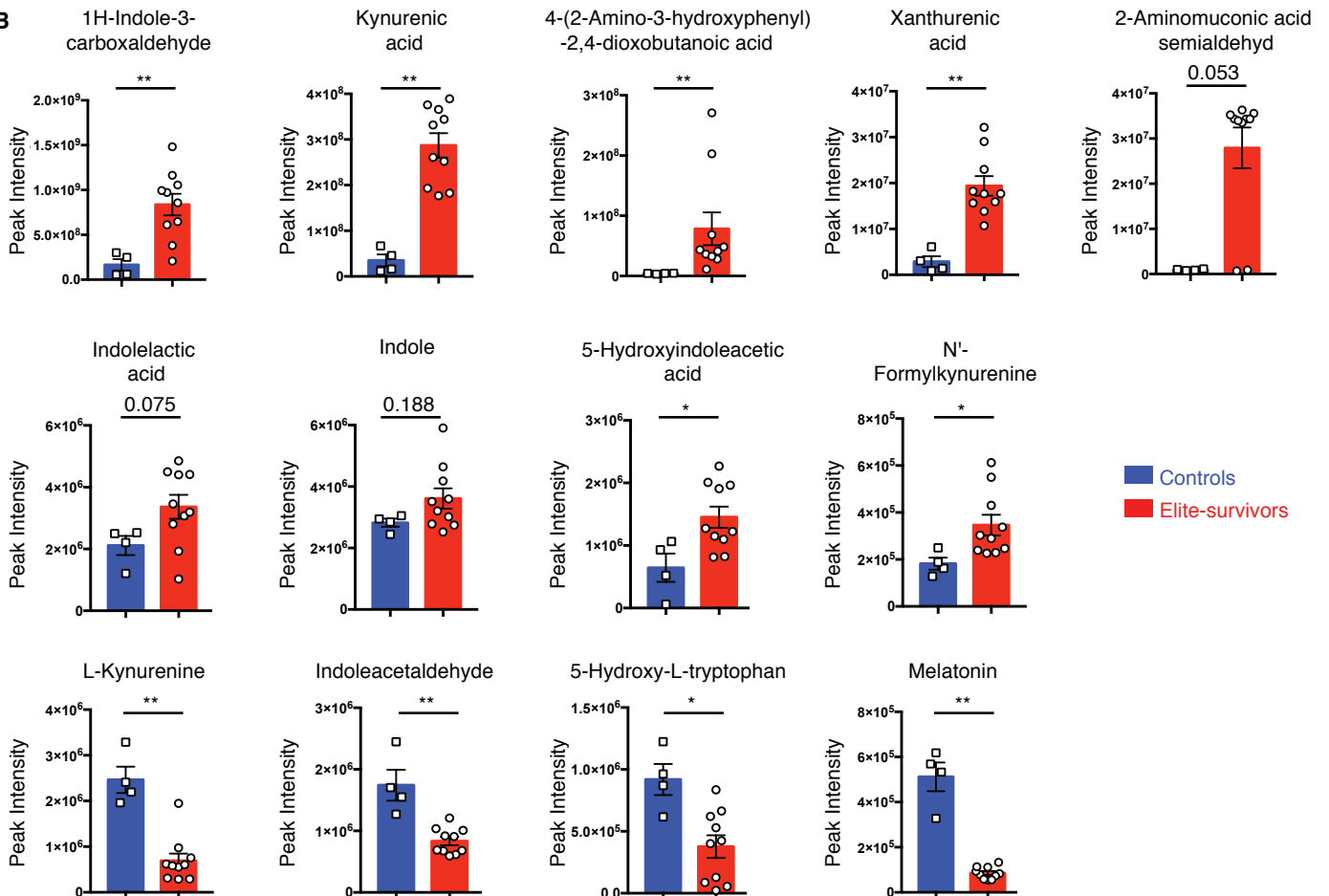
■ Lachno-SCFA low producer (n=7)
● Lachno-SCFA high producer (n=8)



A



B



References and Notes

1. M. Hauer-Jensen, J. W. Denham, H. J. Andreyev, Radiation enteropathy: Pathogenesis, treatment and prevention. *Nat. Rev. Gastroenterol. Hepatol.* **11**, 470–479 (2014).
[doi:10.1038/nrgastro.2014.46](https://doi.org/10.1038/nrgastro.2014.46) [Medline](#)
2. A. K. Shadad, F. J. Sullivan, J. D. Martin, L. J. Egan, Gastrointestinal radiation injury: Prevention and treatment. *World J. Gastroenterol.* **19**, 199–208 (2013). [doi:10.3748/wjg.v19.i2.199](https://doi.org/10.3748/wjg.v19.i2.199) [Medline](#)
3. A. L. Kau, P. P. Ahern, N. W. Griffin, A. L. Goodman, J. I. Gordon, Human nutrition, the gut microbiome and the immune system. *Nature* **474**, 327–336 (2011). [doi:10.1038/nature10213](https://doi.org/10.1038/nature10213) [Medline](#)
4. P. A. Crawford, J. I. Gordon, Microbial regulation of intestinal radiosensitivity. *Proc. Natl. Acad. Sci. U.S.A.* **102**, 13254–13259 (2005). [doi:10.1073/pnas.0504830102](https://doi.org/10.1073/pnas.0504830102) [Medline](#)
5. M. A. Ciorba, T. E. Riehl, M. S. Rao, C. Moon, X. Ee, G. M. Nava, M. R. Walker, J. M. Marinshaw, T. S. Stappenbeck, W. F. Stenson, Lactobacillus probiotic protects intestinal epithelium from radiation injury in a TLR-2/cyclo-oxygenase-2-dependent manner. *Gut* **61**, 829–838 (2012).
[doi:10.1136/gutjnl-2011-300367](https://doi.org/10.1136/gutjnl-2011-300367) [Medline](#)
6. A. Wang, Z. Ling, Z. Yang, P. R. Kiela, T. Wang, C. Wang, L. Cao, F. Geng, M. Shen, X. Ran, Y. Su, T. Cheng, J. Wang, Gut microbial dysbiosis may predict diarrhea and fatigue in patients undergoing pelvic cancer radiotherapy: A pilot study. *PLOS ONE* **10**, e0126312 (2015).
[doi:10.1371/journal.pone.0126312](https://doi.org/10.1371/journal.pone.0126312) [Medline](#)
7. T. E. Riehl, D. Alvarado, X. Ee, A. Zuckerman, L. Foster, V. Kapoor, D. Thotala, M. A. Ciorba, W. F. Stenson, *Lactobacillus rhamnosus* GG protects the intestinal epithelium from radiation injury through release of lipoteichoic acid, macrophage activation and the migration of mesenchymal stem cells. *Gut* **68**, 1003–1013 (2019). [doi:10.1136/gutjnl-2018-316226](https://doi.org/10.1136/gutjnl-2018-316226) [Medline](#)
8. C. Manichanh, E. Varela, C. Martinez, M. Antolin, M. Llopis, J. Doré, J. Giralt, F. Guarner, J.-R. Malagelada, The gut microbiota predispose to the pathophysiology of acute postradiotherapy

- diarrhea. *Am. J. Gastroenterol.* **103**, 1754–1761 (2008). [doi:10.1111/j.1572-0241.2008.01868.x](https://doi.org/10.1111/j.1572-0241.2008.01868.x) [Medline](#)
9. Y. S. Kim, J. Kim, S. J. Park, High-throughput 16S rRNA gene sequencing reveals alterations of mouse intestinal microbiota after radiotherapy. *Anaerobe* **33**, 1–7 (2015). [doi:10.1016/j.anaerobe.2015.01.004](https://doi.org/10.1016/j.anaerobe.2015.01.004) [Medline](#)
10. L. Chen, J. E. Wilson, M. J. Koenigsnecht, W.-C. Chou, S. A. Montgomery, A. D. Truax, W. J. Brickey, C. D. Packey, N. Maharshak, G. K. Matsushima, S. E. Plevy, V. B. Young, R. B. Sartor, J. P.-Y. Ting, NLRP12 attenuates colon inflammation by maintaining colonic microbial diversity and promoting protective commensal bacterial growth. *Nat. Immunol.* **18**, 541–551 (2017). [doi:10.1038/ni.3690](https://doi.org/10.1038/ni.3690) [Medline](#)
11. A. E. Reeves, M. J. Koenigsnecht, I. L. Bergin, V. B. Young, Suppression of *Clostridium difficile* in the gastrointestinal tracts of germfree mice inoculated with a murine isolate from the family Lachnospiraceae. *Infect. Immun.* **80**, 3786–3794 (2012). [doi:10.1128/IAI.00647-12](https://doi.org/10.1128/IAI.00647-12) [Medline](#)
12. N. Reichardt, S. H. Duncan, P. Young, A. Belenguer, C. McWilliam Leitch, K. P. Scott, H. J. Flint, P. Louis, Phylogenetic distribution of three pathways for propionate production within the human gut microbiota. *ISME J.* **8**, 1323–1335 (2014). [doi:10.1038/ismej.2014.14](https://doi.org/10.1038/ismej.2014.14) [Medline](#)
13. P. M. Smith, M. R. Howitt, N. Panikov, M. Michaud, C. A. Gallini, M. Bohlooly-Y, J. N. Glickman, W. S. Garrett, The microbial metabolites, short-chain fatty acids, regulate colonic Treg cell homeostasis. *Science* **341**, 569–573 (2013). [doi:10.1126/science.1241165](https://doi.org/10.1126/science.1241165) [Medline](#)
14. N. Arpaia, C. Campbell, X. Fan, S. Dikiy, J. van der Veecken, P. deRoos, H. Liu, J. R. Cross, K. Pfeffer, P. J. Coffey, A. Y. Rudensky, Metabolites produced by commensal bacteria promote peripheral regulatory T-cell generation. *Nature* **504**, 451–455 (2013). [doi:10.1038/nature12726](https://doi.org/10.1038/nature12726) [Medline](#)
15. J. H. Kim, R. K. Thimmulappa, V. Kumar, W. Cui, S. Kumar, P. Kombairaju, H. Zhang, J. Margolick, W. Matsui, T. Macvittie, S. V. Malhotra, S. Biswal, NRF2-mediated Notch pathway activation enhances hematopoietic reconstitution following myelosuppressive radiation. *J. Clin. Invest.* **124**, 730–741 (2014). [doi:10.1172/JCI70812](https://doi.org/10.1172/JCI70812) [Medline](#)

16. X. Gao, Q. Cao, Y. Cheng, D. Zhao, Z. Wang, H. Yang, Q. Wu, L. You, Y. Wang, Y. Lin, X. Li, Y. Wang, J.-S. Bian, D. Sun, L. Kong, L. Birnbaumer, Y. Yang, Chronic stress promotes colitis by disturbing the gut microbiota and triggering immune system response. *Proc. Natl. Acad. Sci. U.S.A.* **115**, E2960–E2969 (2018). [doi:10.1073/pnas.1720696115](https://doi.org/10.1073/pnas.1720696115) [Medline](#)
17. M. G. Rooks, W. S. Garrett, Gut microbiota, metabolites and host immunity. *Nat. Rev. Immunol.* **16**, 341–352 (2016). [doi:10.1038/nri.2016.42](https://doi.org/10.1038/nri.2016.42) [Medline](#)
18. M. Levy, E. Blacher, E. Elinav, Microbiome, metabolites and host immunity. *Curr. Opin. Microbiol.* **35**, 8–15 (2017). [doi:10.1016/j.mib.2016.10.003](https://doi.org/10.1016/j.mib.2016.10.003) [Medline](#)
19. N. D. Mathewson, R. Jenq, A. V. Mathew, M. Koenigsnecht, A. Hanash, T. Toubai, K. Oravec-Wilson, S.-R. Wu, Y. Sun, C. Rossi, H. Fujiwara, J. Byun, Y. Shono, C. Lindemans, M. Calafiore, T. M. Schmidt, K. Honda, V. B. Young, S. Pennathur, M. van den Brink, P. Reddy, Gut microbiome-derived metabolites modulate intestinal epithelial cell damage and mitigate graft-versus-host disease. *Nat. Immunol.* **17**, 505–513 (2016). [doi:10.1038/ni.3400](https://doi.org/10.1038/ni.3400) [Medline](#)
20. T. Feehley, C. H. Plunkett, R. Bao, S. M. Choi Hong, E. Culleen, P. Belda-Ferre, E. Campbell, R. Aitoro, R. Nocerino, L. Paparo, J. Andrade, D. A. Antonopoulos, R. Berni Canani, C. R. Nagler, Healthy infants harbor intestinal bacteria that protect against food allergy. *Nat. Med.* **25**, 448–453 (2019). [doi:10.1038/s41591-018-0324-z](https://doi.org/10.1038/s41591-018-0324-z) [Medline](#)
21. G. T. Macfarlane, S. Macfarlane, Bacteria, colonic fermentation, and gastrointestinal health. *J. AOAC Int.* **95**, 50–60 (2012). [doi:10.5740/jaoacint.SGE_Macfarlane](https://doi.org/10.5740/jaoacint.SGE_Macfarlane) [Medline](#)
22. E. E. Canfora, J. W. Jocken, E. E. Blaak, Short-chain fatty acids in control of body weight and insulin sensitivity. *Nat. Rev. Endocrinol.* **11**, 577–591 (2015). [doi:10.1038/nrendo.2015.128](https://doi.org/10.1038/nrendo.2015.128) [Medline](#)
23. M. C. Maa, M. Y. Chang, M.-Y. Hsieh, Y.-J. Chen, C.-J. Yang, Z.-C. Chen, Y. K. Li, C.-K. Yen, R.-R. Wu, T.-H. Leu, Butyrate reduced lipopolysaccharide-mediated macrophage migration by suppression of Src enhancement and focal adhesion kinase activity. *J. Nutr. Biochem.* **21**, 1186–1192 (2010). [doi:10.1016/j.jnutbio.2009.10.004](https://doi.org/10.1016/j.jnutbio.2009.10.004) [Medline](#)

24. L. Liu, L. Li, J. Min, J. Wang, H. Wu, Y. Zeng, S. Chen, Z. Chu, Butyrate interferes with the differentiation and function of human monocyte-derived dendritic cells. *Cell. Immunol.* **277**, 66–73 (2012). [doi:10.1016/j.cellimm.2012.05.011](https://doi.org/10.1016/j.cellimm.2012.05.011) [Medline](#)
25. P. V. Chang, L. Hao, S. Offermanns, R. Medzhitov, The microbial metabolite butyrate regulates intestinal macrophage function via histone deacetylase inhibition. *Proc. Natl. Acad. Sci. U.S.A.* **111**, 2247–2252 (2014). [doi:10.1073/pnas.1322269111](https://doi.org/10.1073/pnas.1322269111) [Medline](#)
26. A. Trompette, E. S. Gollwitzer, K. Yadava, A. K. Sichelstiel, N. Sprenger, C. Ngom-Bru, C. Blanchard, T. Junt, L. P. Nicod, N. L. Harris, B. J. Marsland, Gut microbiota metabolism of dietary fiber influences allergic airway disease and hematopoiesis. *Nat. Med.* **20**, 159–166 (2014). [doi:10.1038/nm.3444](https://doi.org/10.1038/nm.3444) [Medline](#)
27. M. Wlodarska, C. Luo, R. Kolde, E. d’Hennezel, J. W. Annand, C. E. Heim, P. Krastel, E. K. Schmitt, A. S. Omar, E. A. Creasey, A. L. Garner, S. Mohammadi, D. J. O’Connell, S. Abubucker, T. D. Arthur, E. A. Franzosa, C. Huttenhower, L. O. Murphy, H. J. Haiser, H. Vlamakis, J. A. Porter, R. J. Xavier, Indoleacrylic acid produced by commensal *Peptostreptococcus* species suppresses inflammation. *Cell Host Microbe* **22**, 25–37.e6 (2017). [doi:10.1016/j.chom.2017.06.007](https://doi.org/10.1016/j.chom.2017.06.007) [Medline](#)
28. S. Krishnan, Y. Ding, N. Saedi, M. Choi, G. V. Sridharan, D. H. Sherr, M. L. Yarmush, R. C. Alaniz, A. Jayaraman, K. Lee, Gut microbiota-derived tryptophan metabolites modulate inflammatory response in hepatocytes and macrophages. *Cell Rep.* **23**, 1099–1111 (2018). [doi:10.1016/j.celrep.2018.03.109](https://doi.org/10.1016/j.celrep.2018.03.109) [Medline](#)
29. C. J. Kurkjian, H. Guo, N. D. Montgomery, N. Cheng, H. Yuan, J. R. Merrill, G. D. Sempowski, W. J. Brickey, J. P.-Y. Ting, The toll-like receptor 2/6 agonist, FSL-1 lipopeptide, therapeutically mitigates acute radiation syndrome. *Sci. Rep.* **7**, 17355 (2017). [doi:10.1038/s41598-017-17729-9](https://doi.org/10.1038/s41598-017-17729-9) [Medline](#)
30. J. U. Peled, A. L. C. Gomes, S. M. Devlin, E. R. Littmann, Y. Taur, A. D. Sung, D. Weber, D. Hashimoto, A. E. Slingerland, J. B. Slingerland, M. Maloy, A. G. Clurman, C. K. Stein-Thoeringer, K. A. Markey, M. D. Docampo, M. Burgos da Silva, N. Khan, A. Gessner, J. A. Messina, K. Romero, M. V. Lew, A. Bush, L. Bohannon, D. G. Breerton, E. Fontana, L. A.

- Amoretti, R. J. Wright, G. K. Armijo, Y. Shono, M. Sanchez-Escamilla, N. Castillo Flores, A. Alarcon Tomas, R. J. Lin, L. Yáñez San Segundo, G. L. Shah, C. Cho, M. Scordo, I. Politikos, K. Hayasaka, Y. Hasegawa, B. Gyurkocza, D. M. Ponce, J. N. Barker, M.-A. Perales, S. A. Giral, R. R. Jenq, T. Teshima, N. J. Chao, E. Holler, J. B. Xavier, E. G. Pamer, M. R. M. van den Brink, Microbiota as predictor of mortality in allogeneic hematopoietic-cell transplantation. *N. Engl. J. Med.* **382**, 822–834 (2020). [doi:10.1056/NEJMoa1900623](https://doi.org/10.1056/NEJMoa1900623) [Medline](#)
31. A. D. Truax, L. Chen, J. W. Tam, N. Cheng, H. Guo, A. A. Koblansky, W.-C. Chou, J. E. Wilson, W. J. Brickey, A. Petrucelli, R. Liu, D. E. Cooper, M. J. Koenigsnecht, V. B. Young, M. G. Netea, R. Stienstra, R. B. Sartor, S. A. Montgomery, R. A. Coleman, J. P.-Y. Ting, The inhibitory innate immune sensor NLRP12 maintains a threshold against obesity by regulating gut microbiota homeostasis. *Cell Host Microbe* **24**, 364–378.e6 (2018). [doi:10.1016/j.chom.2018.08.009](https://doi.org/10.1016/j.chom.2018.08.009) [Medline](#)
32. X. Zheng, Y. Qiu, W. Zhong, S. Baxter, M. Su, Q. Li, G. Xie, B. M. Ore, S. Qiao, M. D. Spencer, S. H. Zeisel, Z. Zhou, A. Zhao, W. Jia, A targeted metabolomic protocol for short-chain fatty acids and branched-chain amino acids. *Metabolomics* **9**, 818–827 (2013). [doi:10.1007/s11306-013-0500-6](https://doi.org/10.1007/s11306-013-0500-6) [Medline](#)
33. Z. Lai, H. Tsugawa, G. Wohlgemuth, S. Mehta, M. Mueller, Y. Zheng, A. Ogiwara, J. Meissen, M. Showalter, K. Takeuchi, T. Kind, P. Beal, M. Arita, O. Fiehn, Identifying metabolites by integrating metabolome databases with mass spectrometry cheminformatics. *Nat. Methods* **15**, 53–56 (2018). [doi:10.1038/nmeth.4512](https://doi.org/10.1038/nmeth.4512) [Medline](#)